Physics Letters B 686 (2010) 18–22

Contents lists available at ScienceDirect

Physics Letters B

www.elsevier.com/locate/physletb

Superdeformation in asymmetric $N > Z$ nucleus ^{40}Ar

E. Ideguchi [a,*], S. Ota [a], T. Morikawa [b], M. Oshima [c], M. Koizumi [c], Y. Toh [c], A. Kimura [c], H. Harada [c], K. Furutaka [c], S. Nakamura [c], F. Kitatani [c], Y. Hatsukawa [c], T. Shizuma [c], M. Sugawara [d], H. Miyatake [e], Y.X. Watanabe [e], Y. Hirayama [e], M. Oi [f]

[a] Center for Nuclear Study, The University of Tokyo, Wako, Saitama 351-0198, Japan
[b] Department of Physics, Kyushu University, Hakozaki, Fukuoka 812-8581, Japan
[c] Japan Atomic Energy Agency, Tokai, Ibaraki 319-1195, Japan
[d] Chiba Institute of Technology, Narashino, Chiba 275-0023, Japan
[e] Institute of Particle and Nuclear Studies, High Energy Accelerator Research Organization (KEK), 1-1 Oho, Tsukuba, Ibaraki 305-0801, Japan
[f] Institute of Natural Sciences, Senshu University, Tokyo 101-8425, Japan

ARTICLE INFO

Article history:
Received 24 September 2009
Received in revised form 19 January 2010
Accepted 9 February 2010
Available online 13 February 2010
Editor: D.F. Geesaman

Keywords:
Nuclear reaction
^{26}Mg(^{18}O, 2p2n)^{40}Ar
Superdeformed shape
Transition quadrupole moments

ABSTRACT

A rotational band with five γ-ray transitions ranging from 2^+ to 12^+ states was identified in ^{40}Ar. This band is linked through γ transitions from the excited 2^+, 4^+ and 6^+ levels to the low-lying states; this determines the excitation energy and the spin–parity of the band. The deduced transition quadrupole moment of $1.45^{+0.49}_{-0.31} \pm 0.15$ eb indicates that the band has a superdeformed shape. The nature of the band is revealed by cranked Hartree–Fock–Bogoliubov calculations and a multiparticle–multihole configuration is assigned to the band.

Until recently, the nuclear magic numbers have been considered to be robust and durable with respect to the shell structure of atomic nuclei. The nuclear shell model initiated by Mayer and Jensen [1] successfully accounts for the shell structure of nuclei on and near the β-stability line. However, recent experimental studies on neutron-rich nuclei far from the β-stability line have revealed the disappearance of magic numbers (e.g., $N = 8$ [2–5], 20 [6]) and the appearance of new magic numbers (e.g., $N = 16$ [7]). The new $N = 16$ magic number comes from the reduction of the $N = 20$ shell gap. One theoretical explanation [8,9] for this phenomenon is that the attractive monopole part of the tensor force acting between the $\pi d_{5/2}$ and $\nu d_{3/2}$ orbitals reduces the $N = 20$ gap in nuclei with high N/Z ratios.

Another interesting phenomenon discovered in neutron-rich nuclei is the occurrence of a *strongly deformed* ground state in and near the $N = 20$ magic nuclei in the $Z \sim 12$ region, the so-called 'island of inversion' [10]. Here, the intruder two-particle, two-hole (2p–2h) configuration occupying the *fp* shell and the normal 0p–0h configuration in the *sd* shell are inverted in energy, and the 2p–2h configuration dominates in the ground state. This is a new challenge to the nuclear shell model. The most convincing evidence for the large quadrupole collectivity of the nuclei in the 'island of inversion' was the measured low $E(2_1^+)$ energy [11] and high $B(\mathrm{E2})$ strength [6], as well as an enhancement of the binding energy [12]. The experimentally deduced large $B(\mathrm{E2}; 0^+_{\mathrm{g.s.}} \rightarrow 2^+_1)$ value indicates large deformation ($\beta_2 = 0.51(5)$) in ^{32}Mg [6]. ^{34}Mg ($N = 22$) shows an even larger deformation ($\beta_2 = 0.58(6)$) [13]. Monte Carlo shell model calculations [14], which include the effects of the narrowed shell gap at $N = 20$ to invigorate 2p–2h excitations, reproduce the experimental values quite well [13].

On the other hand, such a multiparticle–multihole (mp–mh) excitations appear in the excited states of nuclei near the β-stability line. These states can be studied by heavy-ion induced fusion–evaporation reactions on stable isotopes. In fact, an mp–mh excitation from the *sd* to *fp* shell produces superdeformation in $N = Z$ light mass nuclei, such as ^{36}Ar [15], ^{40}Ca [16], and ^{44}Ti [17]. These superdeformed nuclei exhibit a large deformation of $\beta_2 \sim 0.5$, which is about the same magnitude as the ground state deformation in the 'island of inversion'. The presence of superdeformation in the three above-mentioned nuclei can also be understood in terms of the superdeformed shell gaps of $N = Z = 18$, 20, and 22, respectively [16]. In this region, spherical and superde-

* Corresponding author.
E-mail address: ideguchi@cns.s.u-tokyo.ac.jp (E. Ideguchi).

0370-2693
doi:10.1016/j.physletb.2010.02.031

formed magic numbers occur at similar particle numbers, which results in shape coexistence. However, the existence of a superdeformed shell structure in neutron-rich nuclei has not yet been experimentally confirmed.

In order to access the currently reachable neutron-richest superdeformed states with asymmetric superdeformed magic numbers, especially the nucleus with $N = 22$ corresponding to ^{34}Mg, we employed a proton-emission channel (2p2n) in the fusion–evaporation reaction using the neutron-richest beam and target combination of stable isotopes obtained so far. We successfully populated the high-spin states of the superdeformed double magic $Z = 18$ and $N = 22$ nucleus, ^{40}Ar. In this Letter, we report experimental results on the superdeformed states in ^{40}Ar associated with mp–mh excitations between the *sd* and *fp* shells.

High-spin states in ^{40}Ar have previously been studied by proton–γ coincidence measurements using the ^{37}Cl(α, pγ) reaction [18]. High-spin levels below 6.8 MeV were identified up to (8^+) and spin–parity assignments up to the 6^+ state were obtained from the particle–γ angular correlations. The parity of the 5^- state at 4.494 MeV was determined by the linear polarization of the $5^- \rightarrow 4^+$ transition at 1602 keV. The lifetimes of low-lying levels were measured by the Doppler-shift attenuation method. The high E2 strengths of the $6_2^+ \rightarrow 4_2^+$ and $4_2^+ \rightarrow 2_2^+$ transitions are deduced to be respectively 67^{+38}_{-19} and 46^{+15}_{-10} in Weisskopf units, which indicates the large collectivity of the band. However, the (8^+) assignment was based solely on the similarity of the level structure to that in ^{42}Ca. The γ–γ coincidence relations of the in-band transitions were not examined and the presence of the band structure was not unambiguously identified by experiment. Therefore, it is essential to find the higher-spin members of the rotational band and to confirm the coincidence relations between the in-band γ transitions.

High-spin states in ^{40}Ar were populated via the ^{26}Mg(^{18}O, 2p2n)^{40}Ar reaction with a 70-MeV ^{18}O beam provided by the tandem accelerator facility at the Japan Atomic Energy Agency. Two stacked self-supporting foils of ^{26}Mg enriched isotopes with thicknesses of 0.47 and 0.43 mg/cm^2 were used. The mean beam energy of the ^{18}O beam used to irradiate the ^{26}Mg foils was 69.0 MeV. Gamma rays were measured by the GEMINI-II array [19] consisting of 16 HPGe detectors with BGO Compton suppression shields, in coincidence with charged particles detected by the Si-Ball [20], a 4 π array consisting of 11 ΔE Si detectors that were 170 μm thick. The most forward Si detector was segmented into five sections and the other detectors were segmented into two sections each, giving a total of 25 channels that were used to enhance the selectivity of multi charged-particle events. With a trigger condition of more than two Compton-suppressed Ge detectors firing in coincidence with charged particles, a total number of 6.6×10^8 events were collected.

Based on the number of hits in the charged particle detectors, events were sorted into three types of E_γ–E_γ coincidence matrices for each evaporation channel. A symmetrized matrix was created and the RADWARE program ESCL8R [21] was used to examine the coincidence relations of γ rays. By gating on the previously reported γ rays, high-spin states in ^{40}Ar were investigated.

By gating on the known 1461, 1432, and 571 keV peaks of the $2^+ \rightarrow 0^+$, $4^+ \rightarrow 2^+$, and $6^+ \rightarrow 4^+$ transitions, several new levels were identified above the 5^- states at 4.49 MeV by connecting with high-energy γ transitions of $\geqslant 2.5$ MeV. The previously assigned deformed band members of 2_2^+, 4_2^+, and 6_2^+ states were confirmed at 2.522, 3.515, and 4.960 MeV, respectively. In addition, two γ-ray cascade transitions of 2269 and 2699 keV were identified in coincidence with the 993, 1445, and 1841 keV transitions, which form a rotational band up to the (12^+) state at 11.769 MeV

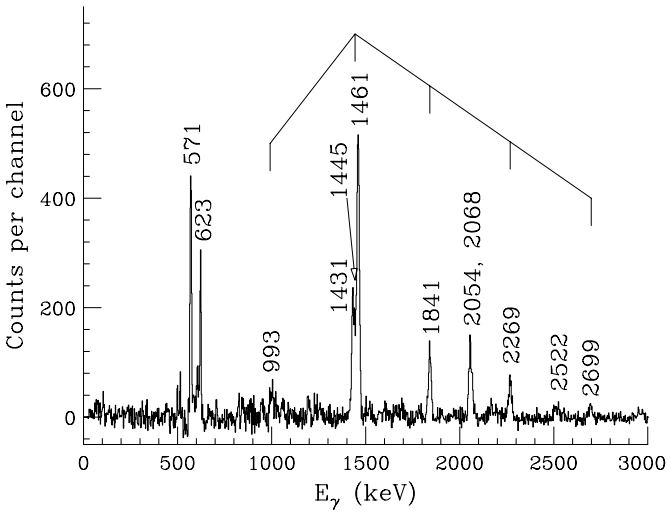

Fig. 1. Gamma-ray energy spectrum created by gating on in-band transition of the superdeformed band in ^{40}Ar.

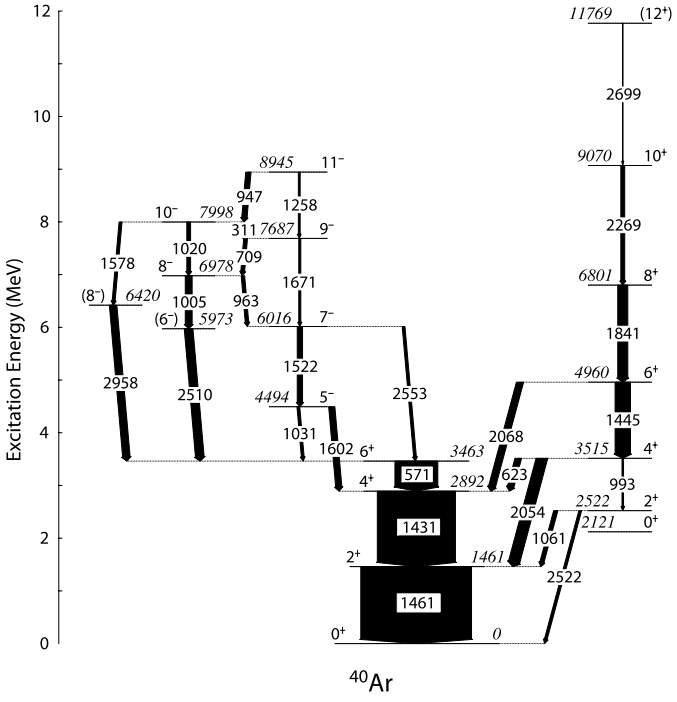

Fig. 2. Partial level scheme of ^{40}Ar constructed in the present study. The width of the arrow of each transition is proportional to its intensity.

(see Fig 1). Linking γ transitions were also observed between the excited 2_2^+, 4_2^+, and 6_2^+ states and the low-lying 2_1^+ and 4_1^+ levels, which establishes the excitation energies and the spin–parity assignment of the band (see Fig 2).

Spins of the observed levels are assigned on the basis of the DCO (Directional Correlations from Oriented states) ratios of γ rays by analyzing an asymmetric angular correlation matrix. The multipolarities of the in-band transitions of the band and the linking transitions of $4_2^+ \rightarrow 2_1^+$ and $6_2^+ \rightarrow 4_1^+$ are consistent with stretched quadrupole character. Assuming E2 multipolarity for the stretched quadrupole transition, the parity of the band was assigned to be positive. The multipolarity of the 2699 keV transition could not be determined due to the lack of statistics, but it was in coincidence with other γ transitions in the band and assigned as E2.

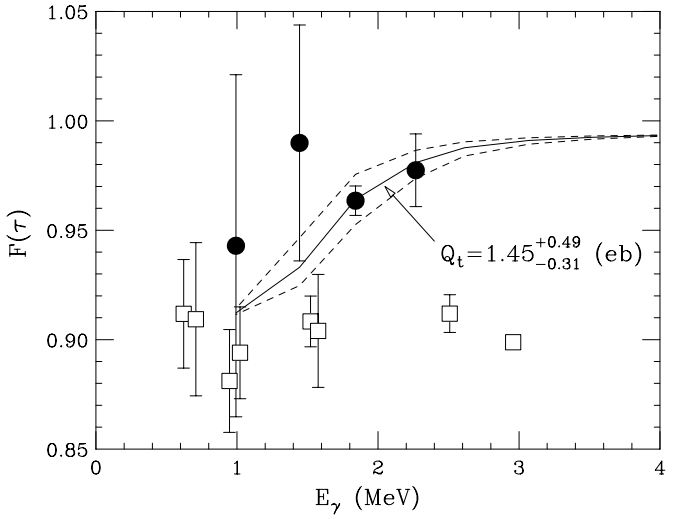

Fig. 3. Fractional Doppler shift $F(\tau)$ as a function of γ-ray energy. Data points for the superdeformed band (filled circles) and other transitions with similar spins (open squares) are extracted from the residual Doppler shift of the γ-ray energies. Solid lines represent the transition quadrupole moment $Q_t = 1.45$ eb and dashed lines correspond to the quoted uncertainties.

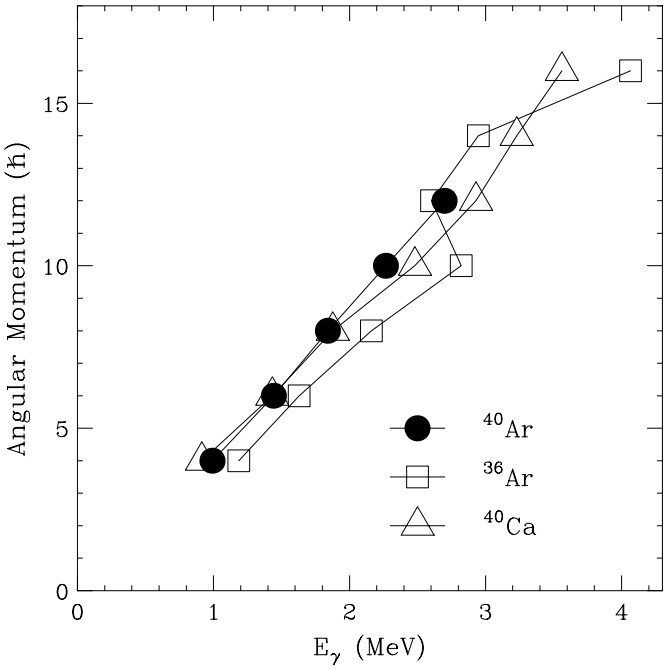

Fig. 4. Backbending plot of the superdeformed bands in ^{36}Ar, ^{40}Ar and ^{40}Ca.

To determine the deformation of the band, the transition quadrupole moment Q_t was deduced. Lifetimes were estimated by the [22] technique, which is based on the residual Doppler shift of the γ-ray energies emitted from the deceleration of recoiling nuclei in a thin target. The average recoil velocity $\langle\beta\rangle$ is expressed as a function of the initial recoil velocity to obtain $F(\tau) \equiv \langle\beta\rangle/\beta_0$. In Fig. 3, the fractional Doppler shift $F(\tau)$ is plotted against the γ-ray energy. The experimental $F(\tau)$ values are compared with the calculated values based on known stopping powers [23]. In this calculation, the side feeding into each state is assumed to consist of a cascade of two transitions having the same lifetime as the in-band transitions. The intensities of the side-feeding transitions were modeled to reproduce the observed intensity profile. The deduced Q_t value for the band could be sensitively correlated with the choice of the side-feeding lifetime. In order to estimate the influences of side-feeding lifetimes, we examined $F(\tau)$ values using two different spectra. They are created by gating above and below the transitions of interest. The data are best fitted with a transition quadrupole moment $Q_t = 1.45^{+0.49}_{-0.31} \pm 0.15$ eb. The second uncertainties quoted are systematic ones due to the influences of side-feeding lifetimes and the uncertainties in the stopping powers ($\sim 10\%$). The deduced Q_t value corresponds to a quadrupole deformation of $\beta_2 \sim 0.5$ assuming a rigid axially symmetric rotor,

$$\beta_2 = \sqrt{\frac{5}{16\pi}}\frac{4\pi\, Q_t}{3R^2 Z},$$

where R denotes the nuclear radius at zero deformation ($R = 1.2A^{1/3}$) and Z is the atomic number. Experimentally deduced Q_t values scaled by $R^2 Z$ for superdeformed bands of ^{36}Ar [15] and ^{40}Ca [16] are 0.40 ± 0.16 and $0.53^{+0.12}_{-0.09}$, respectively. That of ^{40}Ar is deduced to be $0.48^{+0.16}_{-0.10} \pm 0.05$, and it is comparably large as those of ^{36}Ar and ^{40}Ca. This result is consistent with a superdeformed shape of the band in ^{40}Ar.

In order to compare the high-spin behavior of the rotational band in ^{40}Ar with the superdeformed bands in ^{36}Ar and ^{40}Ca, the so-called 'backbending' plot of the superdeformed bands is displayed in Fig. 4. The gradients of the plots correspond to the kinematic moments of inertia. Because ^{40}Ar has a similar gradient to ^{36}Ar and ^{40}Ca, the deformation size of the ^{40}Ar rotational band is expected to be as large as the deformation of the superdeformed bands in ^{36}Ar and ^{40}Ca. Unlike ^{36}Ar, no backbending was observed in ^{40}Ar. Its behavior is rather similar to that of ^{40}Ca. Many theoretical models, including the shell model [15,24–26] and various mean-field models [27–29], have been used to analyze ^{36}Ar. All the calculations reveal that the strong backbending in ^{36}Ar is due to the simultaneous alignment of protons and neutrons in the $f_{7/2}$ orbital.

The pronounced difference in the high-spin behaviors of ^{36}Ar and ^{40}Ar implies that the addition of four neutrons to ^{36}Ar gives rise to a significant effect on its structure. In order to understand this structural change, cranked Hartree–Fock–Bogoliubov (HFB) calculations with the $P + QQ$ force [29] were conducted. The evolution of the nuclear shape was treated in a self-consistent manner and the model space of the full *sd–fp* shell plus the $g_{9/2}$ orbital was employed. The calculation shows that $\beta_2 = 0.57$ at $J = 0\hbar$ and that the deformation gradually decreases to 0.45 at $J = 12\hbar$. Triaxiality is found to be almost zero ($\gamma \simeq 0$) throughout this angular momentum range. This result agrees with the experimental Q_t value within the error bars.

The occupation number of each orbital was also calculated for ^{36}Ar and ^{40}Ar (Table 1). In the shell model, the ground-state configuration of ^{36}Ar is expressed as a four-hole state relative to the ground-state configuration of ^{40}Ca. On the other hand, putting four more neutrons into the above state makes the ground state of ^{40}Ar. In our HFB calculation, the second 0^+ states of ^{36}Ar and ^{40}Ar are shown to be

$$\left|0_2^+\left(^{36}\mathrm{Ar}\right)\right\rangle \sim \pi\left[(d_{5/2})^{-0.9}(s_{1/2}d_{3/2})^{-3.7}(fp)^{2.3}(g_{9/2})^{0.4}\right] \otimes \nu\left[(d_{5/2})^{-0.9}(s_{1/2}d_{3/2})^{-3.7}(fp)^{2.3}(g_{9/2})^{0.4}\right]$$

and

$$\left|0_2^+\left(^{40}\mathrm{Ar}\right)\right\rangle \sim \pi\left[(d_{5/2})^{-1.2}(s_{1/2}d_{3/2})^{-3.8}(fp)^{2.5}(g_{9/2})^{0.5}\right] \otimes \nu\left[(d_{5/2})^{-0.7}(s_{1/2}d_{3/2})^{-2.4}(fp)^{4.5}(g_{9/2})^{0.5}\right],$$

respectively. The former state is interpreted as the so-called "4p–4h" configuration of ^{36}Ar, which is regarded as a superdeformed state [29]. Although the latter state looks similar to the former state, a difference is seen in the occupation number in

Table 1
Occupation numbers of ^{36}Ar [29] (upper part) and ^{40}Ar (lower part) at $J = 0\hbar$ determined by HFB calculation. Holes are denoted by negative numbers.

	Orbital	$d_{5/2}$	$s_{1/2}$	$d_{3/2}$	$f_{7/2}$	$p_{3/2}$	$f_{5/2}$	$p_{1/2}$	$g_{9/2}$
^{36}Ar	Proton	−0.93	−0.97	−2.77	1.46	0.61	0.12	0.11	0.38
	Neutron	−0.93	−0.97	−2.77	1.40	0.65	0.12	0.12	0.36
^{40}Ar	Proton	−1.19	−1.05	−2.74	1.53	0.70	0.15	0.13	0.46
	Neutron	−0.65	−0.39	−2.02	2.88	0.95	0.44	0.27	0.53

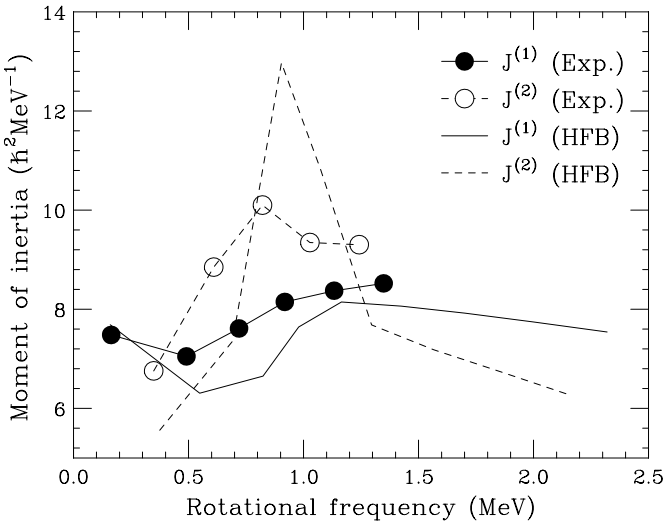

Fig. 5. Kinematical ($J^{(1)}$) and dynamical ($J^{(2)}$) moments of inertia of ^{40}Ar plotted as a function of rotational frequency.

the subspace of $\nu[(s_{1/2}d_{3/2})(fp)]$. The difference can be easily understood by considering that putting four more neutrons into $|0_2^+(^{36}\mathrm{Ar})\rangle$ as done in the ground state. In other words, $|0_2^+(^{40}\mathrm{Ar})\rangle$ can be considered as a kind of "4p–4h" excitation from the ground state of ^{40}Ar.

Cranking is then performed to study high-spin states. Fig. 5 shows experimental and calculated kinematical ($J^{(1)}$) and dynamical ($J^{(2)}$) moments of inertia for ^{40}Ar as a function of rotational frequency. As shown in the figure, our HFB calculations reproduced both magnitudes and behaviors of $J^{(1)}$ and $J^{(2)}$ values reasonably well. In Fig. 6, occupation numbers for each orbital are plotted as a function of total angular momentum. In the proton sector, the behaviors of single-particle occupation are similar to those of ^{36}Ar [29]. For example, the occupation numbers in the $\pi p_{3/2}$ orbital monotonically decrease up to $J = 16\hbar$ while the $\pi f_{7/2}$ orbital starts to increase at $J = 8\hbar$ due to the disappearance of the pairing gap energy. A drop of $J^{(2)}$ values at ~ 0.8 MeV ($J \sim 8\hbar$) might reflect this attenuation of pairing effect.

In the neutron sector, clear differences are observed from the ^{36}Ar case. The occupation number in the $\nu f_{7/2}$ orbital is almost constant ($\sim$3) against the total angular momentum; it is about 1.5 times larger than that for ^{36}Ar. The $\nu d_{5/2}$ orbitals are almost fully occupied ($\simeq 5.5$) from the low- to the high-spin regions. In the case of ^{36}Ar, the structural change involving the sharp backbending is caused by a particle being excited from the $p_{3/2}$ orbital to the $f_{7/2}$ orbital for both protons and neutrons. In the neutron sector of ^{40}Ar, this excitation happens from the $p_{3/2}$ to the many other single-particle orbitals. This is because the rise of the neutron Fermi level enhances the occupation numbers of the single-particle orbitals, particularly at the bottom end of the *fp* shell. For example, the $f_{7/2}$ is well occupied by $\simeq 40\%$. This high occupation influences the response of the system to the Coriolis force. In general, low-Ω states tend to come down energetically lower, so that such states are the first to be "submerged" when the Fermi level rises. As a result, neutron states near the Fermi level in ^{40}Ar possess a higher

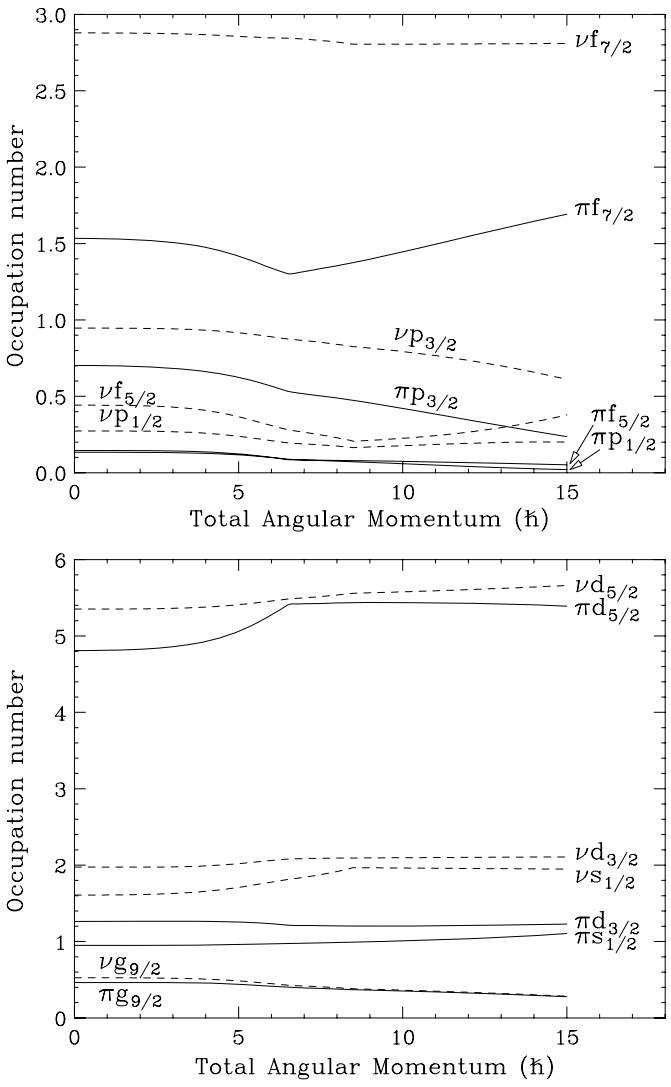

Fig. 6. Occupation numbers for negative-parity (upper panel) and positive-parity (lower panel) orbitals by HFB calculations.

Ω value and the rotational alignment is suppressed. In ^{36}Ar, many $\Omega = 1/2$ states are vacant in the *fp* shell. It is thus possible to place particles in the $\Omega = 1/2$ states when the excitation happens from the $p_{3/2}$ orbital to the $f_{7/2}$ orbital. However, in ^{40}Ar, such $\Omega = 1/2$ states are filled due to the rise of the neutron Fermi level. It is thus necessary to place neutrons in the $\Omega = 3/2$ or 5/2 levels in order to generate angular momentum. But this way of excitation weakens the rotational alignment. This "Pauli blocking effect" is one of the reasons why ^{40}Ar does not backbend (at least, not in the spin region so far observed). It is also worth mentioning that because of the rise of the neutron Fermi level in ^{40}Ar, angular momentum generation is spread among the extra $f_{7/2}$ neutrons, in comparison with ^{36}Ar. This means that, unlike their neutron counterparts, the $f_{7/2}$ protons do not need to "work hard" to generate angular mo-

mentum. As a result, simultaneous alignment of the $f_{7/2}$ protons and neutrons does not occur in ^{40}Ar. Our calculation confirms this picture.

In summary, a superdeformed band has been identified in ^{40}Ar through discrete γ transitions. The observed large transition quadrupole moment ($Q_t = 1.45^{+0.49}_{-0.31} \pm 0.15$ eb) supports its superdeformed character. The properties of the superdeformed band could be reasonably well explained by cranked HFB calculations with the $P + QQ$ force. This finding of the superdeformed band in ^{40}Ar is similar to those observed in ^{36}Ar [15] and ^{40}Ca [16], indicating the persistence of the superdeformed shell structure in the neutron-rich $A = 30$–40 nuclei. As is predicted in Fig. 4 of Ref. [16], the onset of superdeformation in ^{40}Ar might be associated with the superdeformed shell gap at $\beta_2 \sim 0.5$ in $Z = 18$ and $N = 22$. The observed superdeformed structure with a deformation of $\beta_2 \sim 0.5$, caused by the mp–mh excitations across the *sd*–*fp* shell gap, might explain the origin of the strongly deformed ground state in the 'island of inversion'.

Acknowledgements

The authors thank the staff at the JAEA tandem accelerator for providing the ^{18}O beam.

References

[1] M.G. Mayer, Phys. Rev. 75 (1949) 1969;
O. Haxel, J.H.D. Jensen, H.E. Suess, Phys. Rev. 75 (1949) 1766.
[2] A. Navin, et al., Phys. Rev. Lett. 85 (2000) 266.
[3] H. Iwasaki, et al., Phys. Lett. B 481 (2000) 7.
[4] H. Iwasaki, et al., Phys. Lett. B 491 (2000) 8.
[5] S. Shimoura, et al., Phys. Lett. B 560 (2003) 31.
[6] T. Motobayashi, et al., Phys. Lett. B 346 (1995) 9.
[7] A. Ozawa, T. Kobayashi, T. Suzuki, K. Yoshida, I. Tanihata, Phys. Rev. Lett. 84 (2000) 5493.
[8] T. Otsuka, et al., Phys. Rev. Lett. 87 (2001) 082502.
[9] Y. Utsuno, T. Otsuka, T. Glasmacher, T. Mizusaki, M. Honma, Phys. Rev. C 70 (2004) 044307.
[10] E.K. Warburton, J.A. Becker, B.A. Brown, Phys. Rev. C 41 (1990) 1147.
[11] C. Détraz, et al., Phys. Rev. C 19 (1979) 164.
[12] C. Détraz, et al., Nucl. Phys. A 394 (1983) 378.
[13] H. Iwasaki, et al., Phys. Lett. B 522 (2001) 227.
[14] Y. Utsuno, T. Otsuka, T. Mizusaki, M. Honma, Phys. Rev. C 60 (1999) 054315.
[15] C.E. Svensson, et al., Phys. Rev. Lett. 85 (2000) 2693;
C.E. Svensson, et al., Phys. Rev. C 63 (2001) 061301(R).
[16] E. Ideguchi, et al., Phys. Rev. Lett. 87 (2001) 222501.
[17] C.D. O'Leary, et al., Phys. Rev. C 61 (2000) 064314.
[18] E. Bitterwolf, et al., Z. Phys. A 313 (1983) 123.
[19] M. Oshima, et al., J. Radio. Nucl. Chem. 278 (2008) 257.
[20] T. Kuroyanagi, et al., Nucl. Instrum. Methods Phys. Res. Sect. A 316 (1992) 289.
[21] D.C. Radford, Nucl. Instrum. Methods Phys. Res. Sect. A 351 (1995) 297.
[22] B. Cederwall, et al., Nucl. Instrum. Methods Phys. Res. Sect. A 354 (1995) 591.
[23] J.F. Ziegler, J.P. Biersack, U. Littmark, The Stopping and Ranges of Ions in Matter, vol. 1, Pergamon, London, 1985.
[24] E. Caurier, F. Nowacki, A. Poves, Phys. Rev. Lett. 95 (2005) 042502.
[25] E. Caurier, J. Menedéz, F. Nowacki, A. Poves, Phys. Rev. C 75 (2007) 054317;
A. Poves, Nucl. Phys. A 731 (2004) 339.
[26] G.-L. Long, Y. Sun, Phys. Rev. C 63 (2001) 021305(R).
[27] T. Inakura, et al., Nucl. Phys. A 710 (2002) 261.
[28] M. Bender, H. Flocard, P.-H. Heenen, Phys. Rev. C 68 (2003) 044321.
[29] M. Oi, Phys. Rev. C 76 (2007) 044308.